

Some characteristics of elastic waves in a piezoelectric semiconductor plate

EP

Cite as: J. Appl. Phys. 126, 125701 (2019); doi: 10.1063/1.5116662

Submitted: 27 June 2019 · Accepted: 4 September 2019 ·

Published Online: 23 September 2019



View Online



Export Citation



CrossMark

Ru Tian,¹ Jinxi Liu,^{2,3,a)} Ernian Pan,⁴ Yuesheng Wang,^{1,a)} and Ai Kah Soh⁵

AFFILIATIONS

¹Institute of Engineering Mechanics, Beijing Jiaotong University, Beijing 100044, People's Republic of China²Department of Engineering Mechanics, Shijiazhuang Tiedao University, Shijiazhuang 050043, People's Republic of China³Hebei Key Laboratory of Mechanics of Intelligent Materials and Structures, Shijiazhuang Tiedao University, Shijiazhuang 050043, People's Republic of China⁴Department of Civil Engineering, University of Akron, Akron, Ohio 44325-3905, USA⁵School of Engineering, Monash University Malaysia, Jalan Lagoon Selatan, 47500 Bandar Sunway, Selangor Darul Ehsan, Malaysia^{a)}Authors to whom correspondence should be addressed: liujx02@hotmail.com and yswang@tju.edu.cn

ABSTRACT

Devices based on piezoelectric semiconductors (PSCs) have recently received particular attention due to their wide bandgap where strain energy band engineering under both static and time-harmonic deformations is the key. In this paper, we investigate and characterize the elastic waves propagating in an anisotropic n-type PSC plate. To achieve our goals, we first introduce the new notations for the extended displacements, stresses, strains, and modulus to arrive at a mathematically elegant extended Stroh formalism. Then, the elastic wave problem is converted into a linear eigenvalue system from which the extended displacements and stresses are expressed in terms of the eigenvalues and eigenvectors. Finally, making use of the boundary conditions on the top and bottom surfaces of the plate, wave dispersion and attenuation are derived analytically. Numerical examples are presented to systematically study the effect of the surface boundary condition, steady-state carrier density, plate thickness, and biasing electric field on the wave speed and attenuation of both shear horizontal and Lamb waves in the transversely isotropic ZnO PSC plate. Some interesting characteristics of the elastic waves observed in this paper could be helpful as theoretical guidance when designing PSC-based devices.

Published under license by AIP Publishing. <https://doi.org/10.1063/1.5116662>

I. INTRODUCTION

Due to its wide bandgap, piezoelectric (PE) zinc oxide (ZnO) can be used in various semiconductor devices.^{1–3} Furthermore, since ZnO is also piezoelectric, it has the physical properties of both semiconductor and piezoelectric materials.^{4,5} As such, it can be used to make, for instance, acoustic wave amplification devices,^{6–8} nanogenerator,^{9,10} energy harvester,¹¹ and acoustic charge transport devices.^{12,13} In these devices, the wave propagation is essential.

Hutson and White⁴ demonstrated that, due to the interaction between PE and semiconductor (SC), the elastic wave in the piezoelectric semiconductors is both dispersive and damping, a key characteristic of PSCs. The amplification of the (ultrasonic and surface) elastic wave in a PSC can be achieved by applying a dc electric field.^{6,14} For the n-type PSC, the effect of SC characteristic and

biasing electric field on the dispersion and amplification of thickness-shear waves in a single layer PSC plate was investigated.¹⁵ The extensional waves in layered PSC plates¹⁶ and shear horizontal (SH) waves in a semi-infinite PSC¹⁷ were also studied. In addition, the influence of steady-state carrier density and the biasing electric field on the reflection and transmission of elastic waves in a sandwich PSC slab was investigated by Jiao *et al.*¹⁸ The dispersion and attenuation curves of an elastic wave in a semi-infinite p-type PSC space were presented by Jiao *et al.*¹⁹ Since the acoustoelectric effect and amplification of acoustic wave can be achieved by combining the PE effect with the SC characteristic in PSC materials,^{20,21} understanding wave propagation in PSC composites is important. The propagation and amplification of antiplane gap waves between a semi-infinite ceramic and a SC film and SH wave in a SC/PE/SC three-layer plate were all studied recently.^{22–24} The acoustic

diffusive surface waves in the PE layer over a semi-infinite SC²⁵ and the acoustic diffusive waves in the PE/SC/PE three-layer structure²⁶ were presented. Surface acoustic waves in III-V and II-VI SCs were also studied.²⁷ However, so far, all the PSC materials involved in these studies are transverse isotropic or cubic. Furthermore and more importantly, a systematic study on the effect of plate thickness, steady-state carrier density, electrically boundary conditions and biasing electric field on the wave speed and attenuation is missing. This motivates the present research.

In this paper, we investigate and characterize the wave propagation features in a three-dimension n-type PSC plate. To achieve our goal, we first introduce the extended notations to define the extended displacements, stresses, strains, and modulus so that the wave propagation problem is converted to a concise eigenvalue problem in terms of the extended elegant Stroh formalism. Then, in terms of the eigenvalues and eigenvectors, we obtain the general solutions for the extended displacements and stresses. Finally, making use of the boundary conditions on the plate surfaces, the dispersion and attenuation relations are obtained. Numerical examples are carried out to show the influences of the boundary conditions, steady-state carrier density, plate thickness as well as the biasing electric field on the dispersion and attenuation curves. This paper is organized as follows: In Sec. II, we describe the problem to be solved via the basic equations and boundary conditions.

In Sec. III, we derive the dispersion relations. In Sec. IV, various numerical examples are presented and analyzed. Conclusions are drawn in Sec. V.

II. PROBLEM STATEMENTS WITH THE BASIC EQUATIONS

Let us consider an anisotropic n-type PSC plate which is horizontally infinite but vertically finite with thickness h , as shown in Fig. 1. The wave is in the horizontal plane and is propagating along the orientation angle θ from the positive x_1 axis.

Using the extended notation introduced by Barnett and Lothe²⁸ for PE material and generalized to magneto-electro-elastic coupling by Pan,²⁹ the constitutive relations of the n-type PSC in terms of the extended notations can be written as

$$\sigma_{ij} = c_{ijkl}\gamma_{ml} + q\mu_{ij}\bar{E}_j u_l \delta_{jl}, \quad (1)$$

where \bar{E}_j is the uniform biasing electric field, $q = 1.602 \times 10^{-19}$ C is the carrier charge constant, repeated lowercase subscripts take the summation from 1 to 3, whilst those of the uppercase subscripts take the summation from 1 to 5, δ is the Kronecker delta, and the extended stresses and strains are defined as

$$\sigma_{ij} = \begin{cases} \sigma_{ij} & (J = j = 1, 2, 3), \\ D_i & (J = 4), \\ J_i & (J = 5), \end{cases} \quad \gamma_{lj} = \begin{cases} \gamma_{ij} = 0.5(u_{i,j} + u_{j,i}) & (I = i = 1, 2, 3), \\ -E_j = \varphi_j & (I = 4), \\ N_j = n_{,j} & (I = 5), \end{cases} \quad (2)$$

where σ_{ij} , D_i , and J_i are the stresses, electric displacements, and electric currents, respectively; γ_{ij} , E_j , and N_j are the strains, electric field, and carrier density gradient, respectively; u_k , φ , and n are the elastic displacements, electric potential, and carrier density, respectively; a subscript comma denotes the partial differentiation with respect to the coordinates. Also in Eq. (1), the extended material coefficients are defined as

$$c_{ijkl} = \begin{cases} c_{ijkl} & (J = M = j, m = 1, 2, 3), \\ e_{ljj} & (J = j = 1, 2, 3; M = 4), \\ 0 & (J = 1, 2, 3, 4; M = 5), \\ e_{ilm} & (J = 4; M = m = 1, 2, 3), \\ -\varepsilon_{il} & (J = M = 4), \\ 0 & (J = 5; M = 1, 2, 3), \\ -qn_0\mu_{il} & (J = 5; M = 4), \\ -qd_{il} & (J = M = 5), \end{cases} \quad (3)$$

where c_{ijkb} , e_{kij} , and ε_{ij} are the elastic, piezoelectric, and dielectric coefficients, respectively; μ_{ij} and d_{ij} are the carrier mobility and

diffusion coefficients, respectively; and n_0 is the steady-state (or initial) carrier density.

The extended displacements are defined as

$$u_I = \begin{cases} u_i & (I = i = 1, 2, 3), \\ \varphi & (I = 4), \\ n & (I = 5). \end{cases} \quad (4)$$

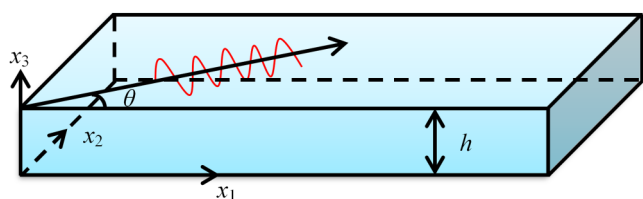


FIG. 1. The geometry of a piezoelectric semiconductor plate with the wave propagation orientation.

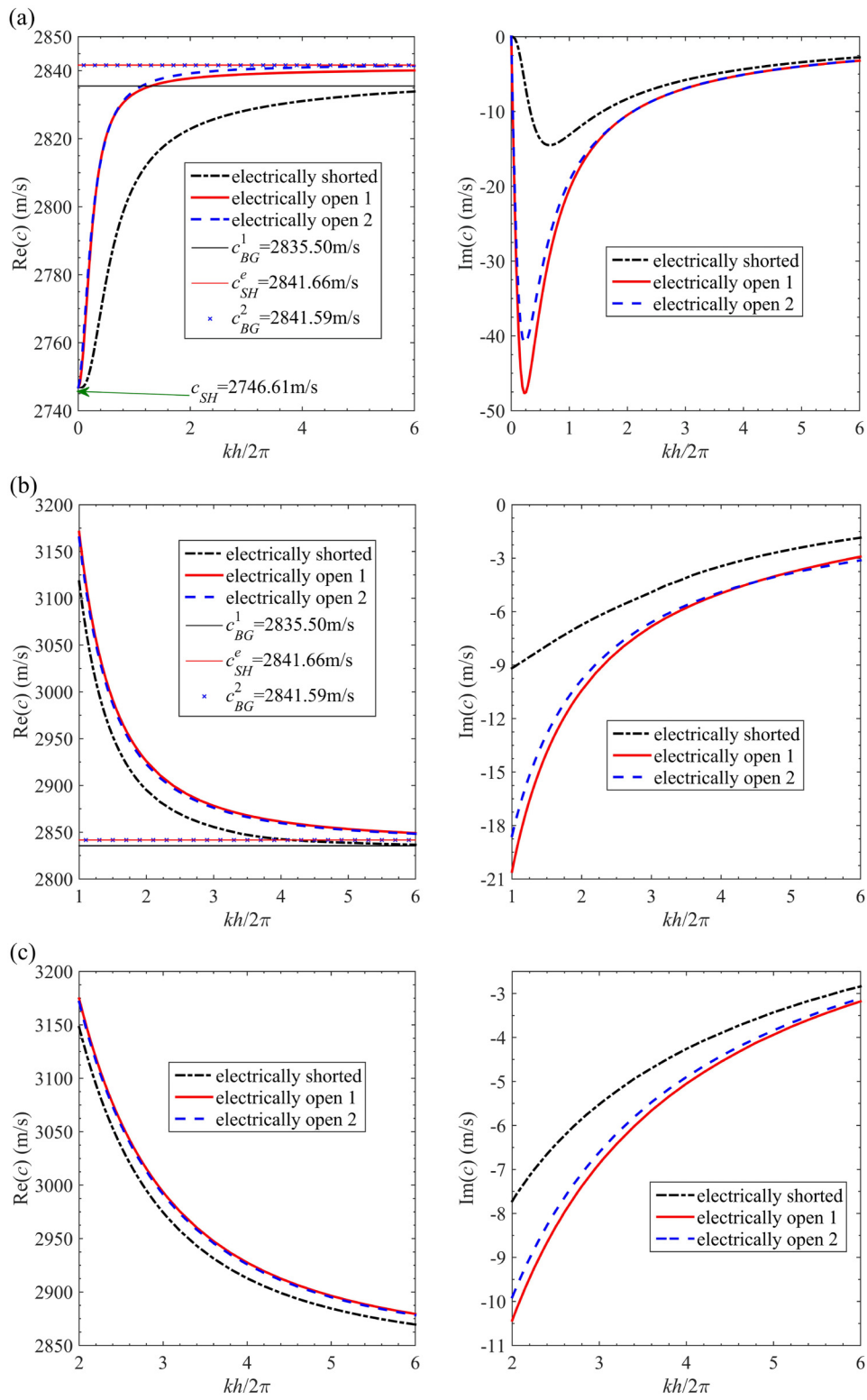


FIG. 2. The lowest three modes with different boundary conditions. (a) The 0th mode, (b) the 1st mode, and (c) the 2nd mode.

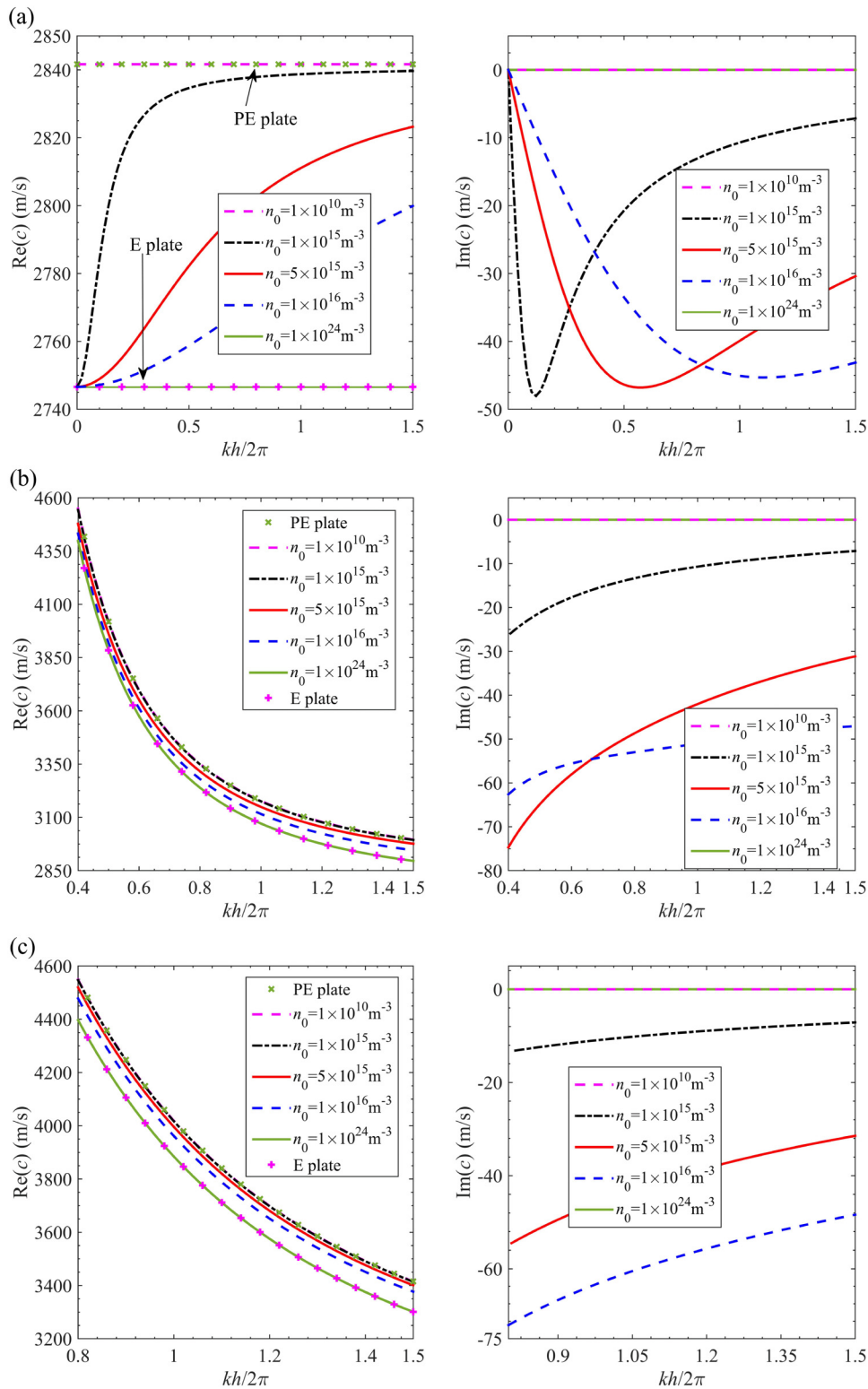


FIG. 3. Dispersion and attenuation curves of the first three modes for different steady-state carrier densities. (a) The 0th mode, (b) the 1st mode, and (c) the 2nd mode.

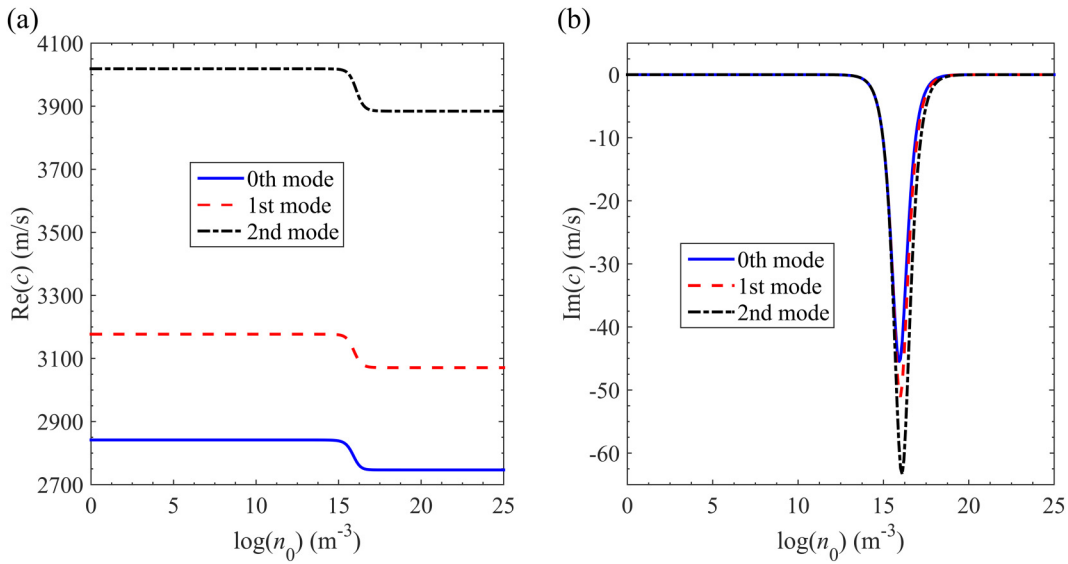


FIG. 4. Wave speed and attenuation of first three modes vs steady-state carrier density for fixed $kh/2\pi = 1$. (a) Wave speed and (b) wave attenuation.

Then, based on these extended notations, the wave equation in the plate can be concisely written as

$$\sigma_{ij,i} = F_j, \quad (5)$$

where

$$F_j = \begin{cases} \rho \ddot{u}_j & (J = j = 1, 2, 3), \\ qn & (J = 4), \\ -qn & (J = 5), \end{cases} \quad (6)$$

in which ρ is the mass density, a dot over a quantity denotes the differentiation with respect to time. We point out that (1) when $q = 0$, the PSC problem is reduced to the corresponding PE problem (by also neglecting the equations related to J_i) and (2) if furthermore, the piezoelectric coefficients $e_{mij} = 0$, then the problem is reduced to the corresponding purely elastic problem (by also neglecting the equations related to D_i). We further emphasize that, due to the involved carrier density in Gauss's law of the electric displacements, both SH and Lamb waves in the homogeneous PSC plate are thickness-dependent. This unique feature is in sharp contrast with that in the corresponding purely elastic or PE plate where waves are independent of the plate thickness.³⁰ Furthermore, while waves in a purely elastic or PE plate are conservative, those in a PSC plate are dissipative.

III. DISPERSION EQUATION

We now define

$$\mathbf{m} = [m_1 \ m_2 \ 0]^T \equiv [\cos \theta \ \sin \theta \ 0]^T, \quad (7)$$

where superscript T denotes the vector or matrix transpose. Then for the wave propagating along the orientation θ within the horizontal plane, the time-harmonic solutions of the extended displacements can be assumed as

$$u_I = a_I e^{ik(x_\gamma m_\gamma - ct)} e^{iskx_3}, \quad (8)$$

where repeated Greek symbol γ takes the summation from 1 to 2; k is the wavenumber; c is the wave speed (or the phase velocity); a_I ($I = 1-5$) are unknown coefficients; and s is the eigenvalue to be determined.

Substituting Eq. (8) into Eq. (1), the generalized traction on the plane perpendicular to the x_3 axis can be found to be

$$\sigma_{3J} = ikb_J e^{ik(x_\gamma m_\gamma - ct)} e^{iskx_3}, \quad (9)$$

where b_J ($J = 1-5$) are the unknown coefficients. Inserting Eqs. (8) and (9) into Eq. (1) yields

$$\mathbf{b} = [\mathbf{R} + s\mathbf{T}] \mathbf{a}, \quad (10)$$

where $\mathbf{a} = [a_1 \ a_2 \ a_3 \ a_4 \ a_5]^T$ is related to the generalized displacement vector, $\mathbf{b} = [b_1 \ b_2 \ b_3 \ b_4 \ b_5]^T$ to the generalized traction vector; and the elements of matrices $[\mathbf{R}]$ and $[\mathbf{T}]$ are

$$R_{JL} = m_\gamma C_{3JL\gamma} + \frac{q\mu_{3j}\bar{E}_j\delta_{J5}}{ik}, \\ T_{JL} = C_{3JL3}. \quad (11)$$

Substituting Eqs. (8)–(9) into Eq. (5) yields

$$[\mathbf{Q} + s(\mathbf{R} + \mathbf{S}) + s^2\mathbf{T}] \mathbf{a} = \mathbf{0}, \quad (12)$$

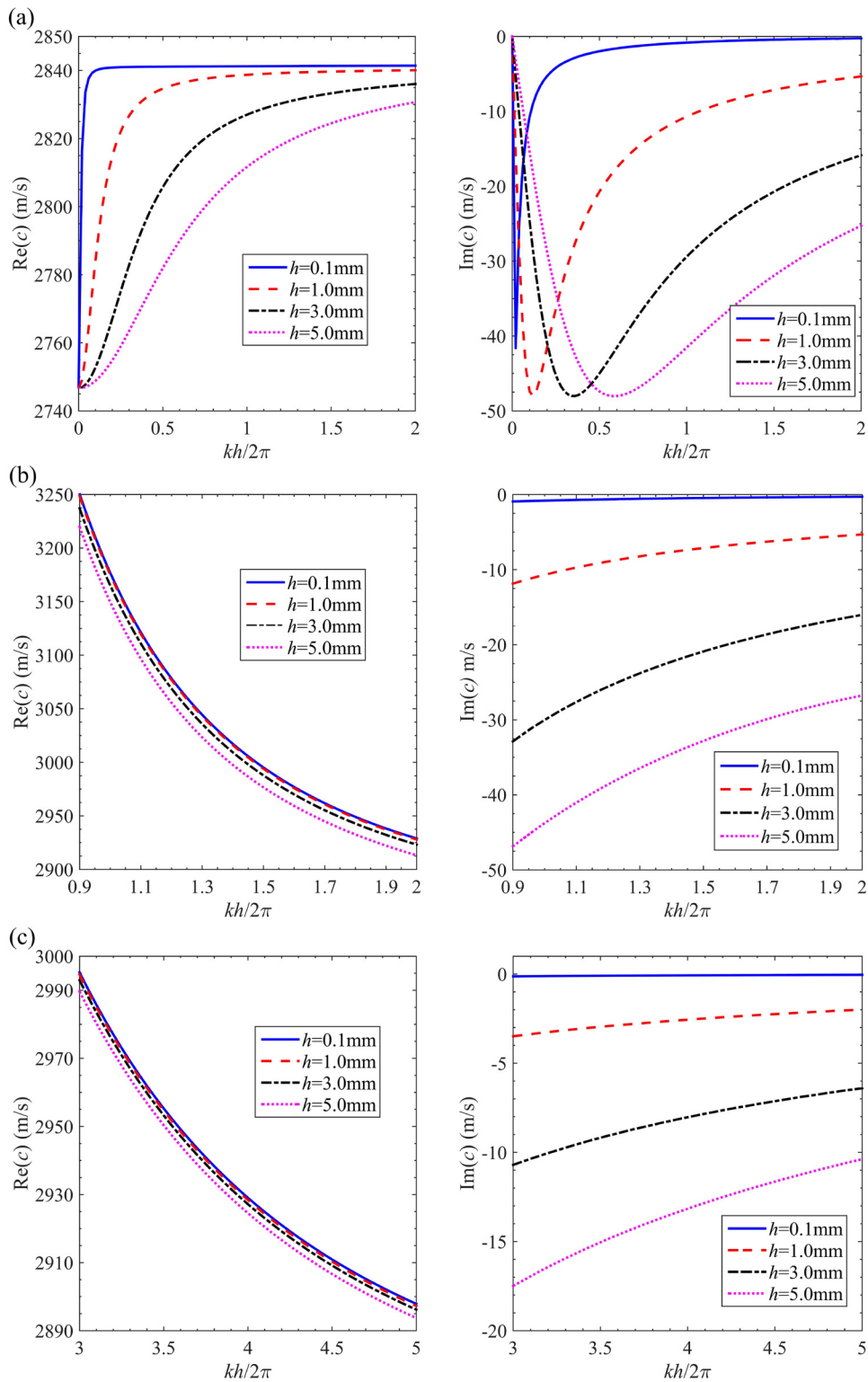


FIG. 5. Dispersion curve for different plate thickness. (a) The 0th mode, (b) the 1st mode, and (c) the 2nd mode.

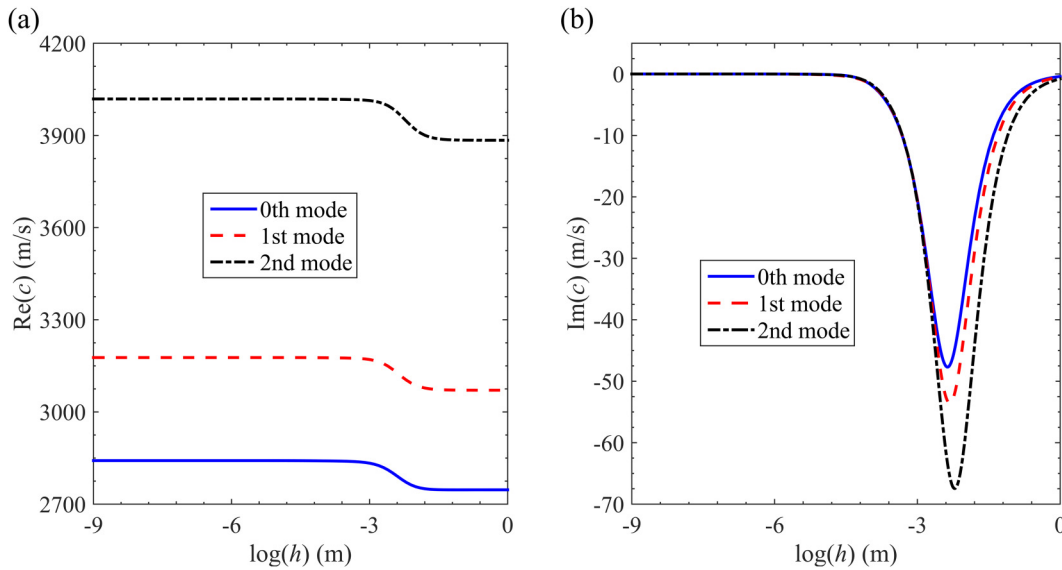


FIG. 6. Wave speed and attenuation of first three modes vs plate thickness for fixed $kh/2\pi = 1$. (a) Wave speed and (b) wave attenuation.

where

$$Q_{JL} = m_\gamma m_\chi C_{\gamma JL\chi} + \frac{q\mu_{\gamma j}\bar{E}_j\delta_{J5}m_\gamma}{ik} + X_{JL}, \quad (13)$$

$$S_{JL} = m_\gamma C_{\gamma JL3},$$

$$X_{JL} = \begin{cases} -\rho c^2 \delta_{jl} & (J=j=1, 2, 3; L=l=1, 2, 3), \\ q/k^2 & (J=4; L=5), \\ -iqc/k & (J=5; L=5), \\ 0 & (J=j=1-3; L=4-5 \text{ or } J=4-5; L=1-3). \end{cases} \quad (14)$$

Then, combining Eqs. (10)–(12), the following linear eigenvalue system can be obtained:

$$[N] \begin{bmatrix} \mathbf{a} \\ \mathbf{b} \end{bmatrix} = s \begin{bmatrix} \mathbf{a} \\ \mathbf{b} \end{bmatrix}, \quad (15)$$

where

$$[N] = \begin{bmatrix} -T^{-1}R & T^{-1} \\ ST^{-1}R - Q & -ST^{-1} \end{bmatrix}. \quad (16)$$

Equation (15) is the extended Stroh formalism (eigenvalue equation) similar to that in magnetoelectroelastic media, which possesses certain mathematical merits.³¹ For instance, conventionally, it is the quadratic-type eigenequation similar to Eq. (12) which was solved in wave analysis in (layered) structures;^{30,32} here, on the other hand, we only need to solve a linear eigenvalue system Eq. (15). Another obvious advantage of applying Eq. (15) is that

not only the displacement eigenvectors but also the traction eigenvectors are the outputs of the eigenvalue system equation (15). Furthermore, Eq. (15) is a unified expression for all the waves and one does not need to derive different expressions corresponding to different types of waves. From Eq. (15), we obtain ten eigenvalues and the corresponding ten eigenvectors \mathbf{a} and \mathbf{b} . Based on them, the general solution of extended displacement and traction vectors can be written as (omitting the proportional coefficient $e^{ik(x_\gamma m_\gamma - ct)}$, and noting also that this general solution includes all the different types of waves, as to be discussed separately below)

$$\begin{bmatrix} ikU(z) \\ T(z) \end{bmatrix} = \begin{bmatrix} E_{11} & E_{12} \\ E_{21} & E_{22} \end{bmatrix} \begin{bmatrix} \langle e^{ik(z-h)s_-} \rangle & \mathbf{0} \\ \mathbf{0} & \langle e^{ikzs_+} \rangle \end{bmatrix} \begin{bmatrix} \mathbf{c}_- \\ \mathbf{c}_+ \end{bmatrix}, \quad (17)$$

where $\mathbf{U} = [u_1 \ u_2 \ u_3 \ \varphi \ n]^T$ is the extended displacement vector, $\mathbf{T} = [\sigma_{31} \ \sigma_{32} \ \sigma_{33} \ D_3 \ J_3]$ is the extended traction vector, $\langle \rangle$ denotes the diagonal matrix of 5×5 . Notice that the ten eigenvalues are ordered as such that $\text{Im}(\mathbf{s}_+) \geq \text{Im}(\mathbf{s}_-)$, and $[E]$ is the eigenmatrix made of the corresponding eigenvectors. The coefficient vectors \mathbf{c}_- and \mathbf{c}_+ can be determined for the given boundary conditions discussed below.

In order to study the wave propagation in the PSC plate, we need the proper boundary conditions on the plate surfaces as considered below.

Mechanically, we assume that both surfaces are traction-free. In other words, on the surfaces, we have (omitting the proportional coefficient $e^{ik(x_\gamma m_\gamma - ct)}$)

$$\sigma_{3i}(x_\gamma, 0) = 0, \quad \sigma_{3i}(x_\gamma, h) = 0, \quad i = 1 \sim 3. \quad (18)$$

As for the electrical boundary condition, the following three cases are considered (omitting the proportional coefficient $e^{ik(x_\gamma m_\gamma - ct)}$):

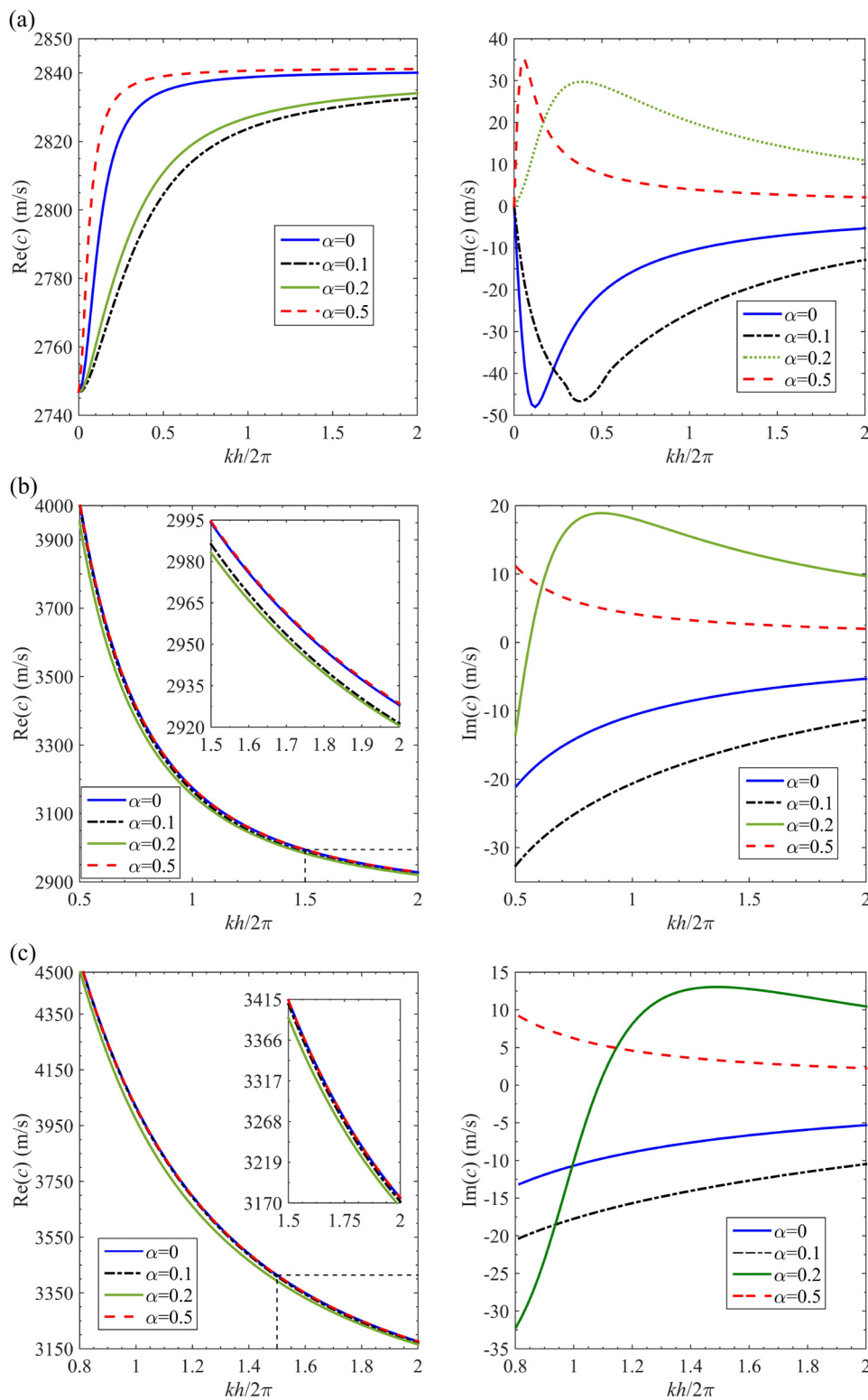


FIG. 7. Effect of dimensionless biasing electric field α on wave speed and attenuation. (a) The 0th mode, (b) the 1st mode ,and (c) the 2nd mode.

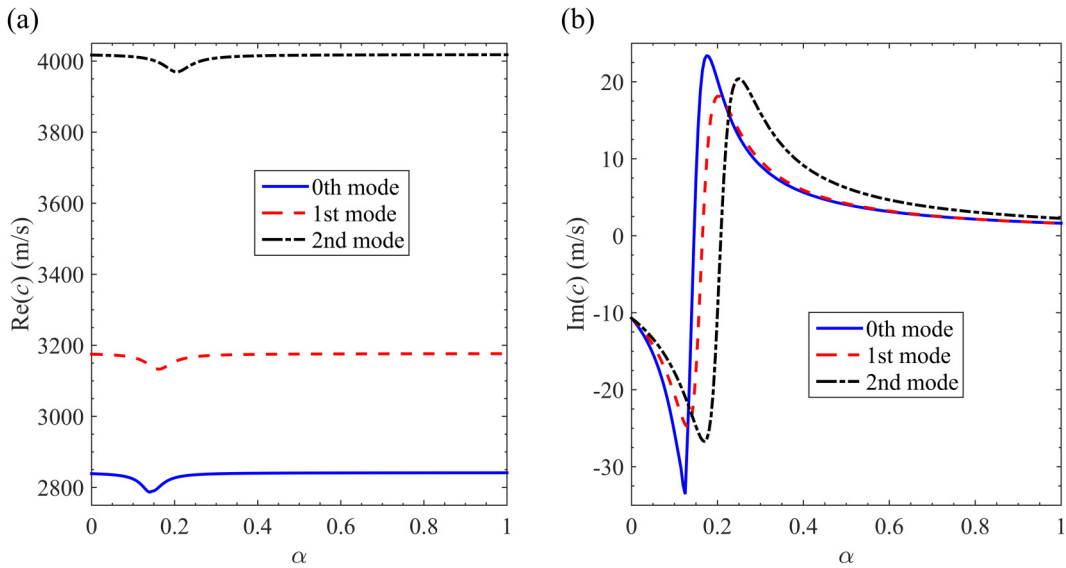


FIG. 8. Wave speed and attenuation of first three modes vs α for $kh/2\pi = 1$. (a) Wave speed and (b) wave attenuation.

A) Electrically shorted (circuit), i.e.,

$$\begin{aligned} \varphi(x_\gamma, 0) &= 0, & n(x_\gamma, 0) &= 0, \\ \varphi(x_\gamma, h) &= 0, & n(x_\gamma, h) &= 0. \end{aligned} \quad (19)$$

B) Electrically open (circuit)¹³³

$$\begin{aligned} -ikcD_3(x_\gamma, 0) + J_3(x_\gamma, 0) &= 0, & n(x_\gamma, 0) &= 0, \\ -ikcD_3(x_\gamma, h) + J_3(x_\gamma, h) &= 0, & n(x_\gamma, h) &= 0. \end{aligned} \quad (20)$$

C) Electrically open (circuit)²¹⁷

$$\begin{aligned} -ikcD_3^-(x_\gamma, 0) + J_3(x_\gamma, 0) &= -ikcD_3^-(x_\gamma, 0), & n(x_\gamma, 0) &= 0, \\ -ikcD_3^+(x_\gamma, h) + J_3(x_\gamma, h) &= -ikcD_3^+(x_\gamma, h), & n(x_\gamma, h) &= 0, \end{aligned} \quad (21)$$

where $D_3^-(x_3 \leq 0)$ and $D_3^+(x_3 \geq h)$ are the electric displacement component in the vacuum.

Substituting Eq. (17) into Eq. (18) and making use of any one of the three different electrical boundary conditions in Eqs. (19)–(21), we obtain a system of homogeneous linear equation for the involved coefficient vectors \mathbf{c}_- and \mathbf{c}_+ ,

$$[\mathbf{M}] \begin{bmatrix} \mathbf{c}_- \\ \mathbf{c}_+ \end{bmatrix} = \mathbf{0}, \quad (22)$$

where $[\mathbf{M}]$ is a 10×10 matrix with its elements listed in Appendix A. In order to obtain a nontrivial solution of the problem, the determinant of the coefficient matrix of Eq. (22) must vanish, which

yields the following dispersion equation:

$$\det [\mathbf{M}] = 0. \quad (23)$$

Therefore, for a given wavenumber k , the wave speed c can be obtained by solving the above equation. The wave speed thus determined is a complex number. Its real and imaginary parts represent the real>true wave speed and attenuation, respectively.

IV. NUMERICAL RESULTS AND DISCUSSION

In this section, we study the propagation characteristics of the SH and Lamb waves in the transversely isotropic ZnO PSC plate. The nonzero material parameters of ZnO are $c_{11} = c_{22} = 210 \text{ GPa}$, $c_{12} = 121 \text{ GPa}$, $c_{13} = 105 \text{ GPa}$, $c_{33} = 211 \text{ GPa}$, $c_{44} = c_{55} = 43 \text{ GPa}$, $c_{66} = 44.5 \text{ GPa}$; $e_{15} = e_{24} = -0.48 \text{ C/m}^2$, $e_{31} = e_{32} = -0.57 \text{ C/m}^2$, $e_{33} = 1.32 \text{ C/m}^2$; $\epsilon_{11} = \epsilon_{22} = 7.61 \times 10^{-11} \text{ C/V m}$, $\epsilon_{33} = 8.85 \times 10^{-11} \text{ C/V m}$; $\rho = 5700 \text{ kg/m}^3$, $d_{11} = d_{22} = d_{33} = 0.026 \text{ m}^2/\text{s}$; and $\mu_{11} = \mu_{22} = \mu_{33} = 1 \text{ m}^2/\text{V}$,^{34,35} the permittivity of vacuum is $\epsilon_0 = 8.854 \times 10^{-12} \text{ C/V m}$. In the following numerical analysis, the nondimensional wavenumber $kh/2\pi$, nondimensional biasing electric fields $\alpha = \bar{E}_1 e_{33}^2 / (qn_0 \mu_{11} c_{11} h)$, $\beta = \bar{E}_3 e_{33}^2 / (qn_0 \mu_{11} c_{11} h)$ are used.

A. SH waves in the piezoelectric semiconductor plate

When the wave is propagating along the x_1 -direction in the transversely isotropic PSC plate, the SH and Lamb waves are decoupled. We thus consider the SH wave first. However, in order to investigate the effect of piezoelectric anisotropy, the x_2 axis (x_3 axis) of the crystal coordinate system is selected to be along the x_3 axis (x_2 axis) of the global plate coordinate system (Fig. 1), different from previous studies where the horizontal plane of the plate is the same as the transversely isotropic plane of the material. For this rotated material

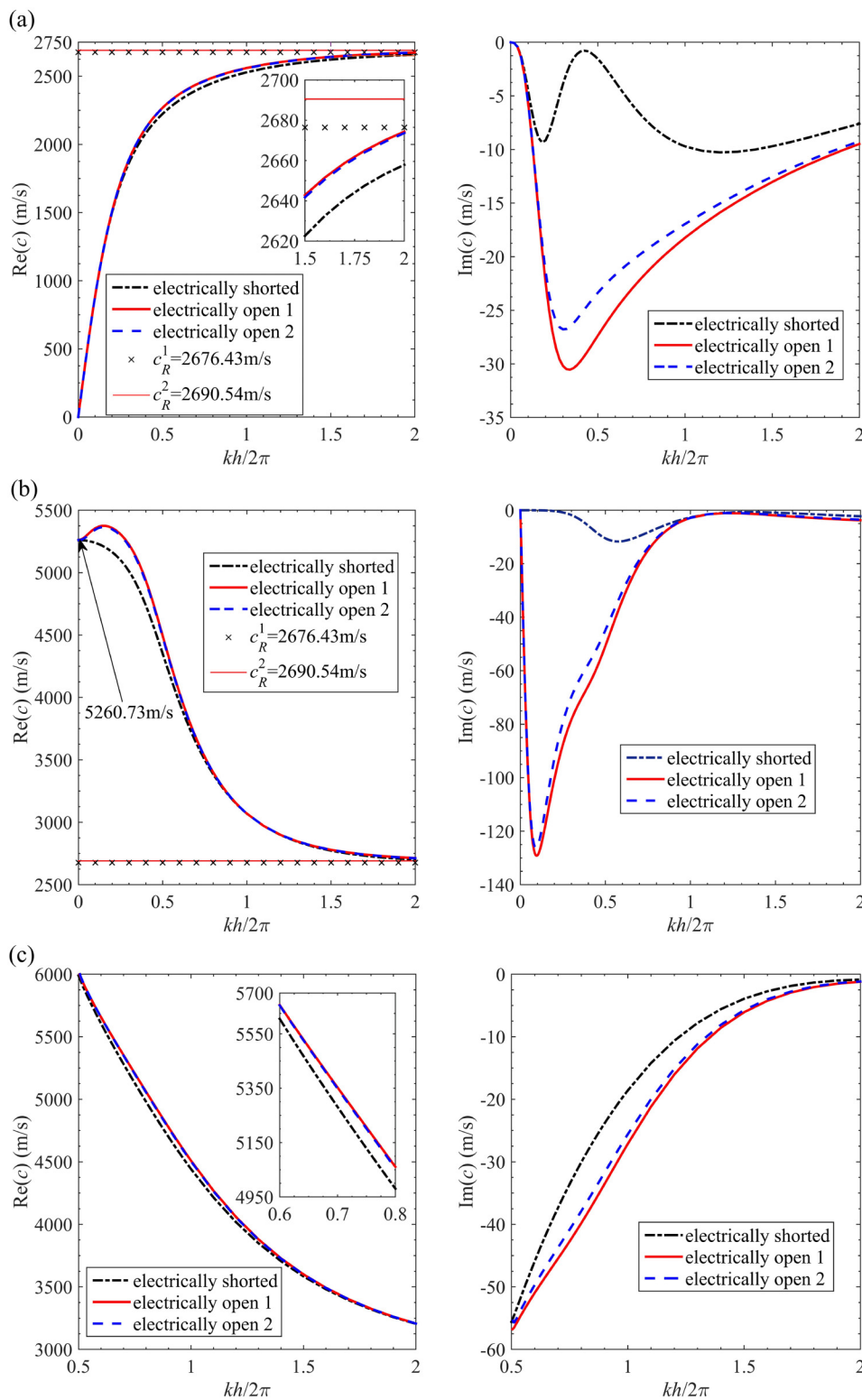


FIG. 9. Effect of the different boundary conditions on the dispersion curves of the first three modes. (a) The 1st mode, (b) the 2nd mode, and (c) the 3rd mode.

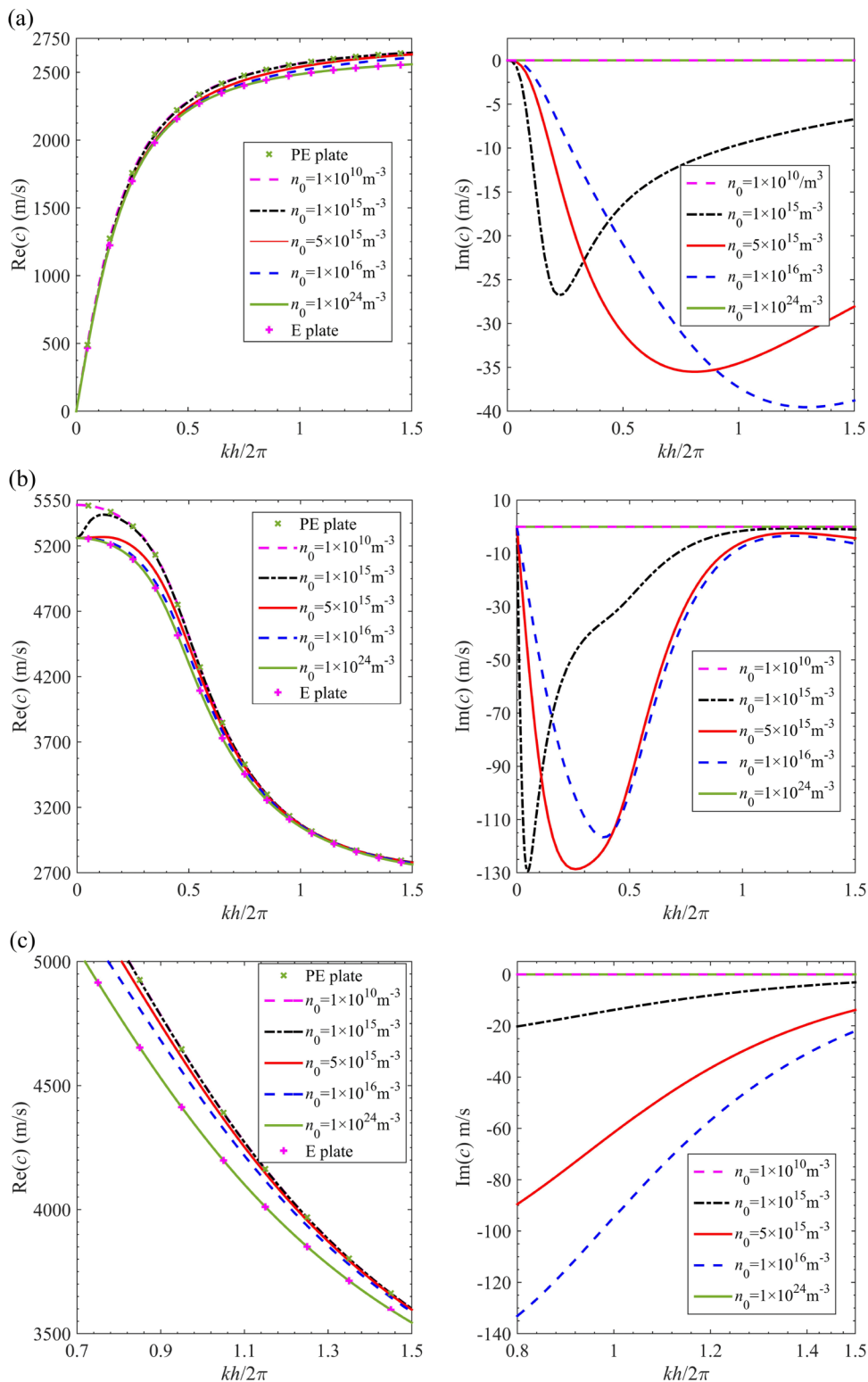


FIG. 10. Dispersion and attenuation curves of the first three modes for different steady-state carrier density. (a) The 1st mode, (b) the 2nd mode, and (c) the 3rd mode.

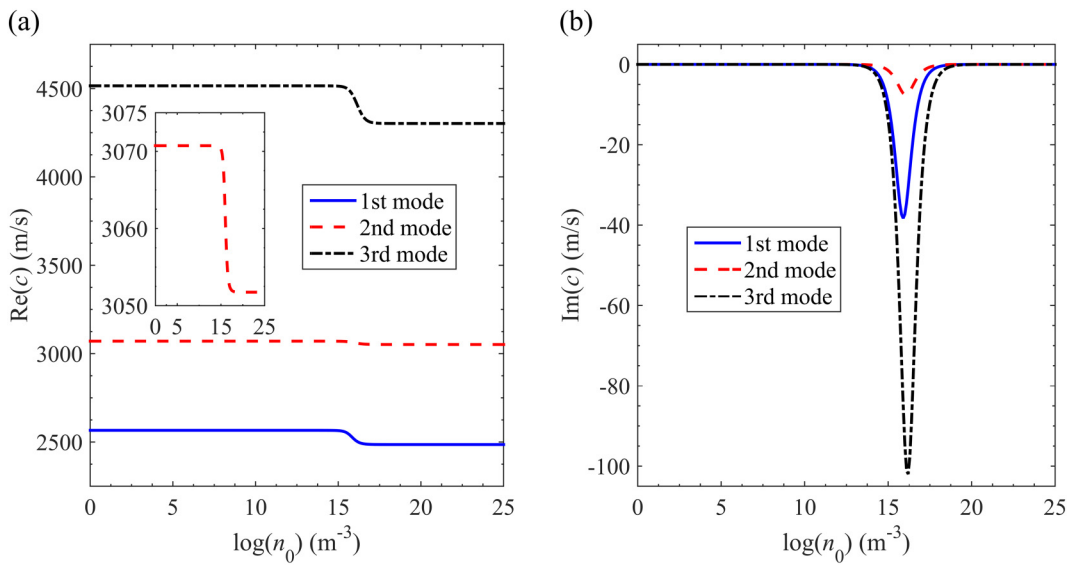


FIG. 11. Variation of the wave speed and attenuation of the first three modes with the steady-state carrier density. (a) Wave speed and (b) wave attenuation.

case, the dispersion relation of the SH wave can be obtained by neglecting the first two rows and two columns and the sixth and seventh rows and the sixth and seventh columns in Eq. (23). Furthermore, for comparison, the body shear-wave speeds of ZnO with and without PE coupling, and the Bleustein-Gulyaev (B-G) wave^{36,37} in the half-space PE ZnO with electrically shorted surface and electrically open surface 2 are also calculated. These wave speeds are defined below. The PE SH and elastic body wave speeds are

$$c_{\text{SH}}^e = \sqrt{\bar{c}_{44}/\rho}, \quad \bar{c}_{44} = c_{44} + e_{15}^2/\varepsilon_{11}, \quad (24)$$

$$c_{\text{SH}} = \sqrt{c_{44}/\rho}. \quad (25)$$

The B-G surface wave speed in the PE half-space is

$$c_{\text{BG}}^l = c_{\text{SH}}^e \sqrt{1 - e_{15}^4/(\varepsilon_{11}^2 \bar{c}_{44}^2)} \quad (26)$$

for the electrically shorted surface and

$$c_{\text{BG}}^o = c_{\text{SH}}^e \sqrt{1 - e_{15}^4 \varepsilon_0^2 / [\bar{c}_{44}^2 \varepsilon_{11}^2 (\varepsilon_0 + \varepsilon_{11})^2]} \quad (27)$$

for the electrically open surface 2.

1. Effect of boundary conditions on wave speed and attenuation

The dispersion and attenuation curves of the first three modes are plotted in Fig. 2. The steady-state carrier density is fixed at $n_0 = 2 \times 10^{15} \text{ m}^{-3}$, and the plate thickness is at $h = 1 \text{ mm}$ with zero

biasing electric fields (i.e., $\bar{E}_1 = \bar{E}_3 = 0$). The following features can be observed from Fig. 2: (1) The wave speed of the zeroth mode begins at the body shear-wave speed c_{SH} for all the three different boundary conditions [Fig. 2(a)]; (2) With increasing wavenumber, the wave speed of the zeroth and first modes approach the speed of the B-G surface wave of PE ZnO for the electrically shorted case and electrically open case 2 [Figs. 2(a) and 2(b)]; (3) With increasing wavenumber, the wave speed of the zeroth and first mode for the electrically open case 1 approaches the body shear-wave speed c_{SH}^e [Figs. 2(a) and 2(b)]; (4) For the three boundary conditions discussed, the imaginary part of phase velocity (or wave speed) c is always negative with much less magnitude as compared to the real part. The imaginary value shows that the wave amplitude is of attenuation instead of growth. Furthermore, for both real and imaginary parts, their magnitude corresponding to the electrically shorted case is usually smaller than that to the electrically opening cases, whilst the magnitudes of both electrically opening cases are very close to each other (at a large value of $kh/2\pi$). As such, in the following calculation, we choose the electrically open case 1 to analyze.

2. Effect of the steady-state carrier density on wave speed and attenuation

Figure 3 shows the dispersion and attenuation curves when $h = 1 \text{ mm}$ and $\bar{E}_1 = \bar{E}_3 = 0$ for different values of the steady-state carrier density n_0 . The green cross and pink plus stand for the wave speeds of SH wave in the corresponding PE and elastic ZnO plate, respectively. From Fig. 3, one can find that (1) when $n_0 = 1 \times 10^{10} \text{ m}^{-3}$, the wave speed of SH wave is equal to the wave speed of the SH wave in the corresponding PE ZnO plate with no attenuation; (2) when $1 \times 10^{15} \text{ m}^{-3} \leq n_0 \leq 1 \times 10^{16} \text{ m}^{-3}$, the wave speed

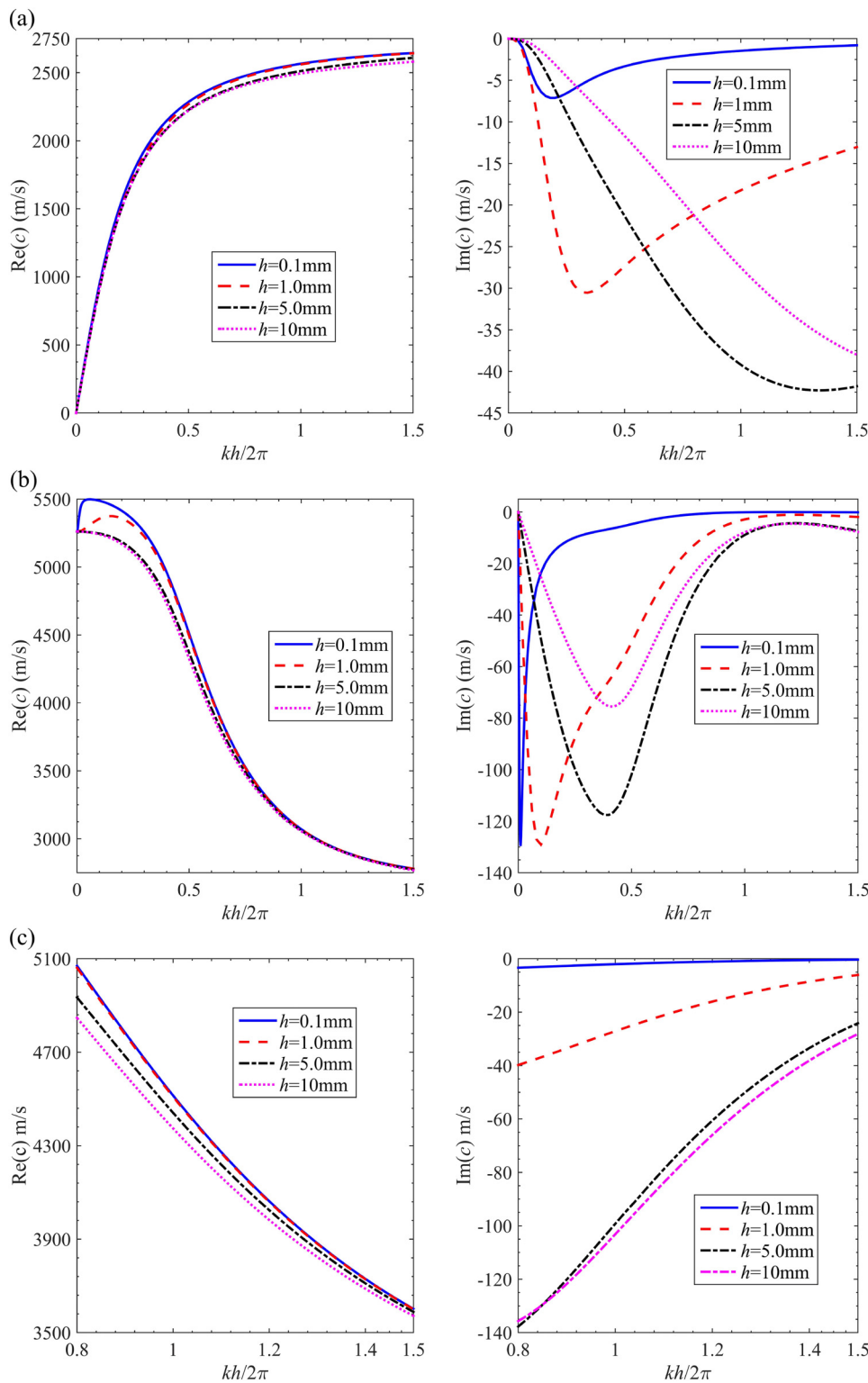


FIG. 12. Wave speed and attenuation against dimensionless wavenumber for different values of h . (a) The 1st mode, (b) the 2nd mode, and (c) the 3rd mode.

decreases with increasing n_0 , and the wave attenuation becomes small for very long waves (i.e., small wavenumber); (3) when $n_0 = 1 \times 10^{24} \text{ m}^{-3}$, the wave speed of SH wave is equal to the wave speed of the SH wave in the corresponding elastic ZnO plate, with no attenuation. It is further observed from Fig. 3(b) that their imaginary part of the wave speed varies strangely with varying n_0 , which is discussed in Fig. 4.

Figure 4 shows the variation of wave speed and attenuation with different n_0 's for fixed $kh/2\pi = 1$, $h = 1 \text{ mm}$ and $\bar{E}_1 = \bar{E}_3 = 0$. The following interesting features can be observed from Fig. 4: (1) when $n_0 < 1 \times 10^{12} \text{ m}^{-3}$, the SH wave propagates with the wave speed of the SH wave in the corresponding PE ZnO plate with zero attenuation; (2) when $1 \times 10^{12} \text{ m}^{-3} \leq n_0 \leq 1 \times 10^{20} \text{ m}^{-3}$, the wave speed decreases with increasing n_0 and approaches the wave speed of the SH wave in the corresponding elastic ZnO plate. Wave attenuation first increases (i.e., with a large amplitude in its imaginary part) and then decreases with increasing n_0 , and finally approaches zero. Therefore, there exists a critical (where the maximum wave attenuation is achieved) $n_0 = 1 \times 10^{15.93} \text{ m}^{-3}$ for the zeroth mode, $n_0 = 1 \times 10^{15.98} \text{ m}^{-3}$ for the first mode, and $n_0 = 1 \times 10^{16.08} \text{ m}^{-3}$ for the second mode. This feature indicates that, in order to design a PSC structure with a large wave amplitude, the steady-state (or initial) carrier density should be away from the critical value; (3) when $n_0 > 1 \times 10^{20} \text{ m}^{-3}$, the SH wave propagates with the wave speed of the SH wave in the corresponding elastic ZnO plate with zero attenuation.

3. Effect of the plate thickness on wave speed and attenuation

The effect of the plate thickness on wave speed and attenuation for fixed $n_0 = 2 \times 10^{15} \text{ m}^{-3}$ and $\bar{E}_1 = \bar{E}_3 = 0$ is shown in

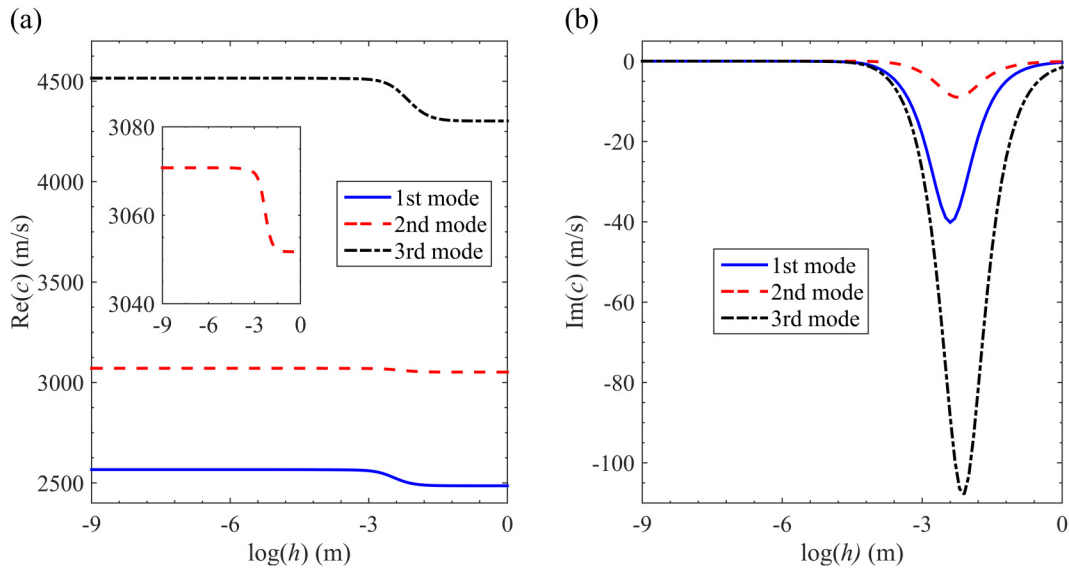


FIG. 13. Wave speed and attenuation of the first three modes vs plate thickness h . (a) Wave speed and (b) wave attenuation.

Fig. 5. It is observed from Fig. 5, different from the SH wave in the corresponding PE plate which is independent of plate thickness, the wave in the PSC plate is now dependent on h . Furthermore, the wave speed decreases with increasing plate thickness. Figure 6 presents the wave speed and attenuation of the first three modes for different plate thicknesses with fixed $kh/2\pi = 1$, $n_0 = 2 \times 10^{15} \text{ m}^{-3}$ and $\bar{E}_1 = \bar{E}_3 = 0$. It is noted that this figure is very similar to Fig. 4 for the variation with respect to n_0 . Here for a given n_0 , with increasing plate thickness, the wave first propagates with the SH wave speed in the corresponding PE ZnO plate and then decrease, and eventually reaches the wave speed of SH wave in the corresponding elastic ZnO plate. As for its wave attenuation, when the plate thickness is increased to certain value, it first increases and then decreases when the plate thickness is continuously increased. Therefore, there exists a critical plate thickness for each mode, i.e., the critical thickness is $h = 4.365 \text{ mm}$ [i.e., $\log(h) = -2.36 \text{ m}$], $h = 4.786 \text{ mm}$ [i.e., $\log(h) = -2.32 \text{ m}$], and $h = 6.166 \text{ mm}$ [i.e., $\log(h) = -2.21 \text{ m}$], respectively, for 0th, 1st, and 2nd modes. As such, once a wave mode is selected for the PSC plate, the critical plate thickness should be avoided.

4. Effect of the biasing electric field on wave speed and attenuation

Since the PSC structure is dissipative with energy being dissipated into the electric current in the system, proper energy input to the system is important. One way to possibly amplify the wave amplitude is by applying a biasing electric field to the PSC devices.^{6,14,38} Recently, the size-effect induced bias field was proposed for high-power terahertz photonic devices.³⁹ Therefore, it is important to analyze the effect of the biasing field on waves in the PSC plate. Figure 7 presents the effect of the biasing (horizontal)

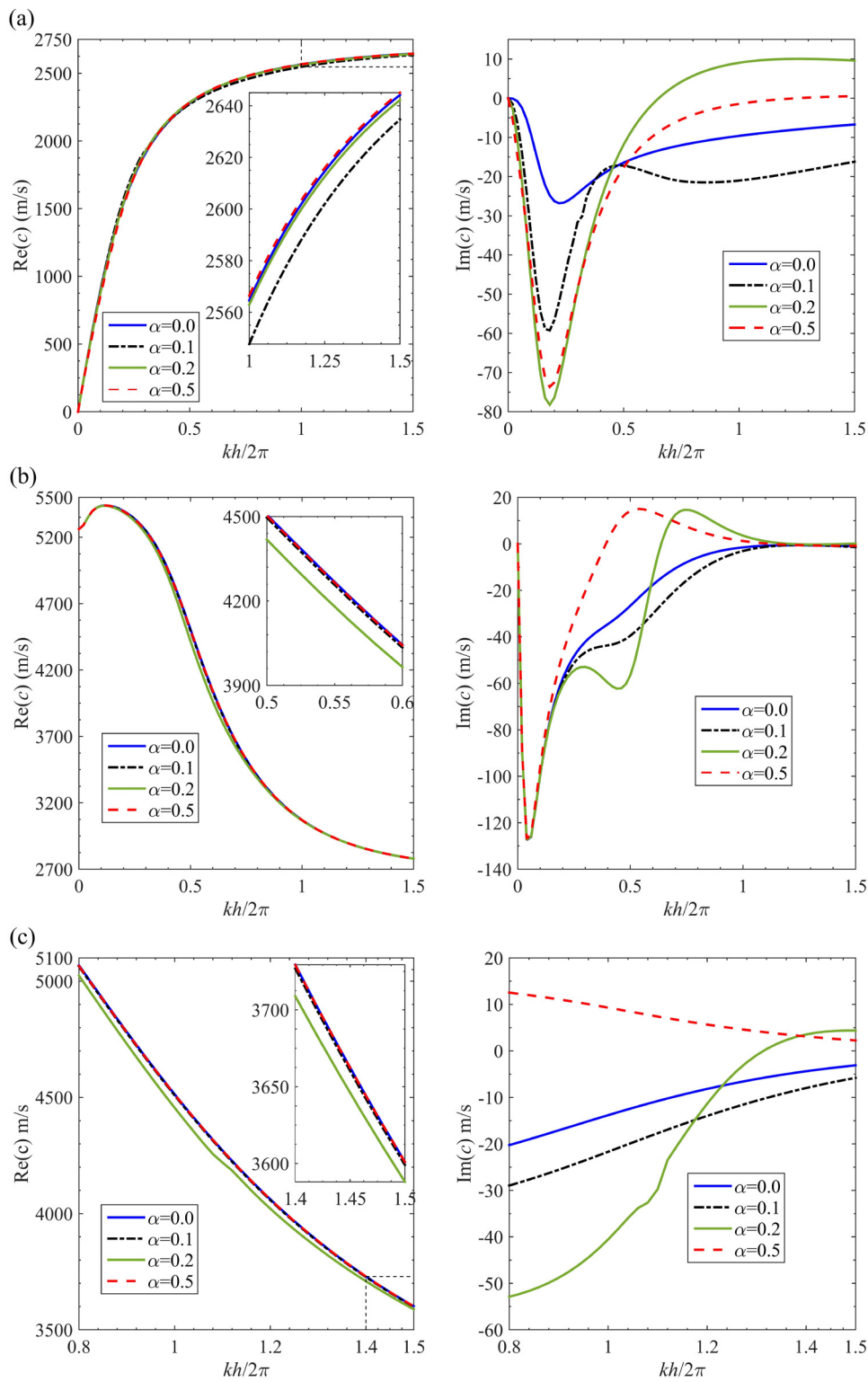


FIG. 14. Dispersion and attenuation curves of the first three modes under different biasing electric field α . (a) The 1st mode, (b) the 2nd mode, and (c) the 3rd mode.

electric field \bar{E}_1 on the wave speed and attenuation with fixed $n_0 = 1 \times 10^{15} \text{ m}^{-3}$, $h = 1 \text{ mm}$, and vertical field $\bar{E}_3 = 0$. It is interesting to observe from Fig. 7, a positive imaginary part of the phase velocity c appears when α is increased to a certain value. This indicates that there exists a wave growth when considering the biasing electric field. This complicated effect of α on c is presented in Fig. 8 for fixed $kh/2\pi = 1$, $n_0 = 1 \times 10^{15} \text{ m}^{-3}$, $h = 1 \text{ mm}$, and $\bar{E}_3 = 0$. It is noted that, with increasing α , the wave speed of first three modes decreases first, then increases, and eventually approaches the SH wave speed in the corresponding PE ZnO plate. The critical α where the minimum wave speed is achieved is at 0.140, 0.162, and 0.205, respectively, for 0th, 1st, and 2nd modes. With increasing α , the wave attenuation increases first, then decreases sharply, and eventually increases again, approaching their limits. When α is larger than a fixed value (e.g., 0.1455 for the 0th mode), the wave attenuation change its sign (so the wave amplitude increases instead of decreasing). The critical α where the maximum wave attenuation is achieved for the first three modes are 0.124, 0.131, and 0.169, respectively. The critical α where the maximum wave growth is achieved is at 0.176, 0.202, and 0.250 for 0th mode, 1st mode, and 2nd mode, respectively. Furthermore, the oscillation feature observed from Fig. 8(b) is consistent with previous experimental and theoretical analyses,^{6,38} and wave growth occurs when the electrons drift velocity exceeds the velocity of the SH wave.⁶ The present result further confirms that it is possible to amplify the ultrasonic wave in a PSC plate by applying a biasing electric field.

B. Lamb wave features in a piezoelectric semiconductor plate

The dispersion and attenuation relations of the Lamb wave in the PSC plate can be obtained by neglecting the second and seventh

rows and the second and seventh columns in Eq. (23). In this analysis, the following special Rayleigh wave speeds of ZnO are provided as references: The Rayleigh wave speeds in the corresponding PE ZnO half-space for the electrically open case 1 $c_R^1 = 2690.54 \text{ m/s}$, and for electrically shorted case $c_R^2 = 2676.43 \text{ m/s}$, and the Rayleigh wave speed in the corresponding elastic ZnO half-space $c_R = 2622.28 \text{ m/s}$.

1. Effect of different boundary conditions on wave speed and attenuation

Figure 9 gives the dispersion and attenuation curves of the first three modes for ZnO plate under three kinds of boundary conditions for fixed $n_0 = 2 \times 10^{15} \text{ m}^{-3}$, $h = 1 \text{ mm}$, and $\bar{E}_1 = \bar{E}_3 = 0$. With increasing wavenumber, the wave speed of first and second modes approaches the Rayleigh wave speed of the corresponding PE ZnO. When $k = 0$, the wave speed of the second mode [Fig. 9(b)] starts at the wave speed of the second Lamb wave in the corresponding PE ZnO plate. The Lamb waves all attenuate for the three kinds of boundary conditions. For the second mode, the imaginary part of c oscillates around the value slightly less than zero. Similar to the SH wave feature, the Lamb wave speed and attenuation for the electrically open cases 1 and 2 are relatively close to each other at a large value of $kh/2\pi$, and thus in the following discussion, we concentrate on the electrically open case 1 only.

2. Effect of steady-state carrier density on wave speed and attenuation

Figure 10 shows the effect of steady-state carrier density on the dispersion and attenuation curves of the first three modes vs wavenumber (for fixed $h = 1 \text{ mm}$ and $\bar{E}_1 = \bar{E}_3 = 0$). The green cross and pink plus stand for the wave speed of Lamb wave in the corresponding ZnO PE plate and ZnO elastic plate, respectively.

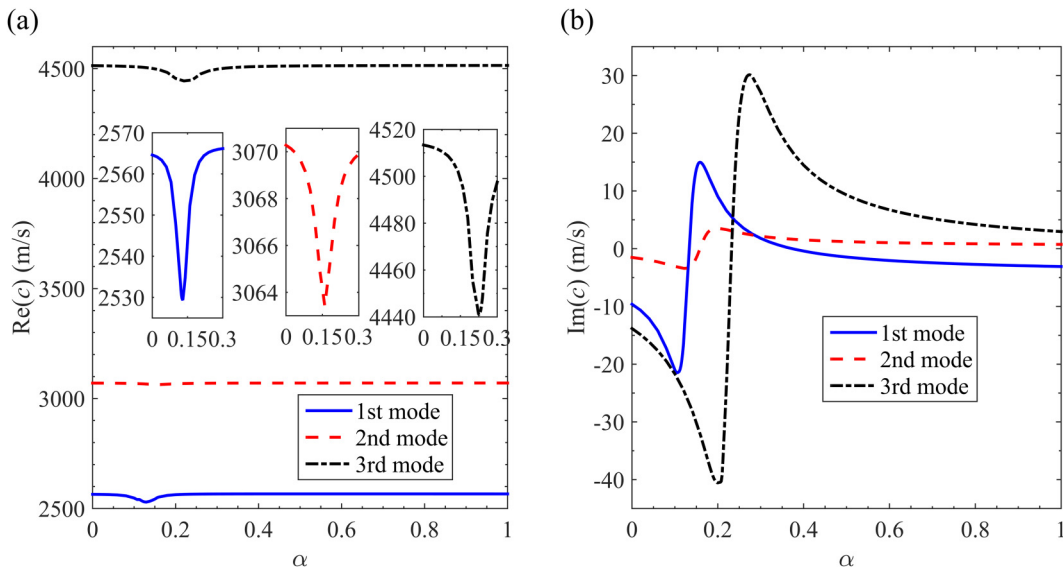


FIG. 15. Variation of wave speed and attenuation of the first three modes against dimensionless horizontal biasing electric field α . (a) Wave speed and (b) wave attenuation.

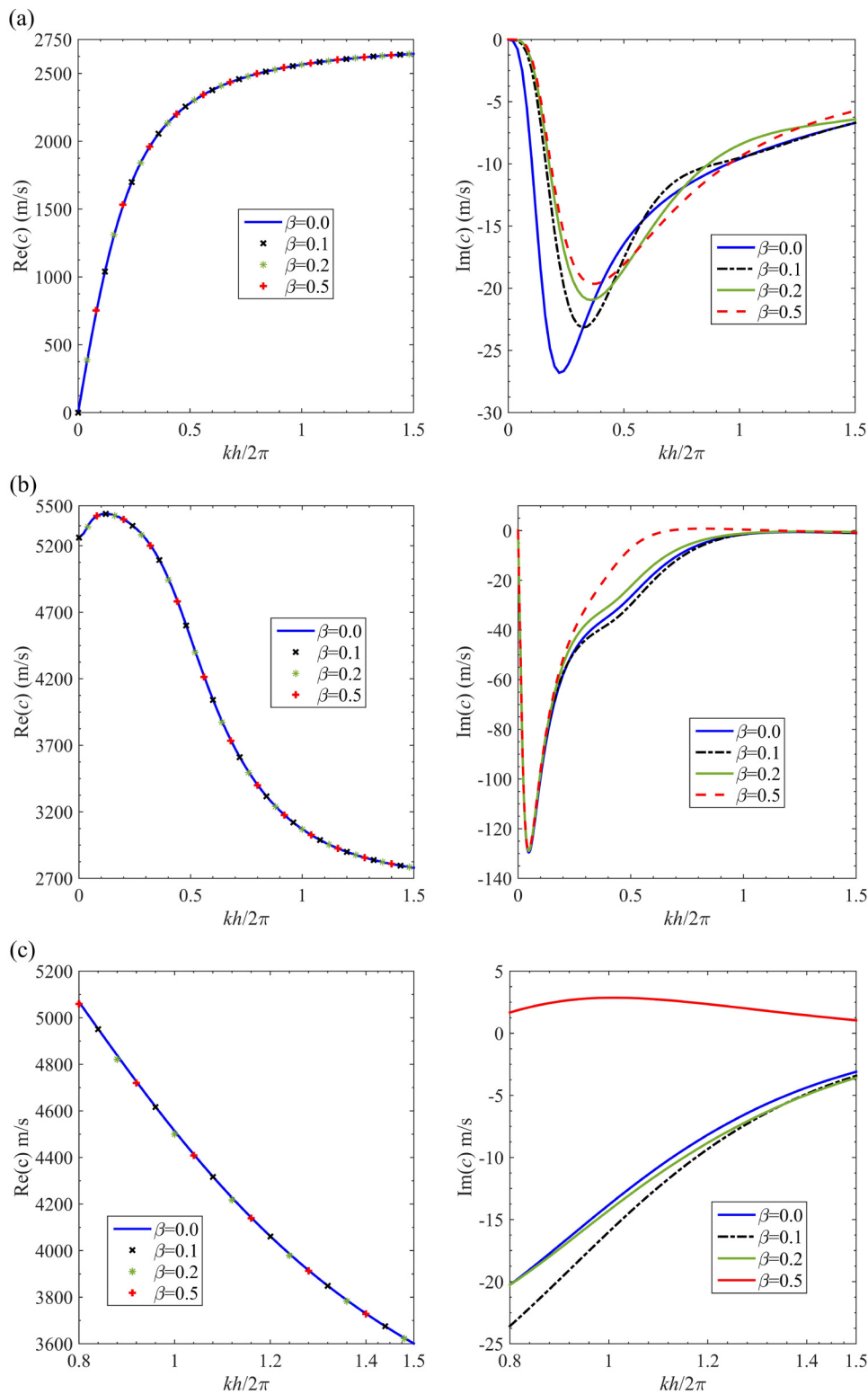


FIG. 16. The lowest three modes with different dimensionless vertical biasing electric field β . (a) The 1st mode, (b) the 2nd mode, and (c) the 3rd mode.

For fixed $kh/2\pi = 1$, the variation of the corresponding wave speed and attenuation vs n_0 is plotted in Fig. 11. From both figures, the following features are observed: (1) when $n_0 < 1 \times 10^{12} \text{ m}^{-3}$, the Lamb wave propagates with the Lamb wave speed in the corresponding piezoelectric ZnO plate with zero attenuation; (2) when $1 \times 10^{12} \text{ m}^{-3} \leq n_0 \leq 1 \times 10^{20} \text{ m}^{-3}$, the wave speed decreases with increasing steady-state carrier density. As for the wave attenuation, it increases first to a critical value; after that, it decreases with increasing n_0 . The critical n_0 for the first, second, and third modes, are respectively, $1 \times 10^{15.89} \text{ m}^{-3}$, $1 \times 10^{16.06} \text{ m}^{-3}$, and $1 \times 10^{16.17} \text{ m}^{-3}$; (3) when $n_0 > 1 \times 10^{20} \text{ m}^{-3}$, the Lamb wave propagates with the Lamb wave speed in the corresponding elastic ZnO plate with zero attenuation. It should be emphasized that, similar to the SH wave in Fig. 4(b), for designing a PSC structure with a large wave amplitude, the critical steady-state (or initial) carrier density should be first identified. The device then should be designed such that its initial carrier density be away from the critical carrier density.

3. Effect of plate thickness on wave speed and attenuation

The dispersion and attenuation curves of the first three modes under different plate thickness are plotted in Fig. 12, for fixed $n_0 = 2 \times 10^{15} \text{ m}^{-3}$ and $\bar{E}_1 = \bar{E}_3 = 0$. It is observed from Fig. 12, when the wavenumber is small, the plate thickness has an obvious effect on the wave speed of the second and third modes; For the first mode, on the contrary, its wave speed is nearly independent of the plate thickness when wavenumber is small, and one can only see the slight effect of the plate thickness when wavenumber becomes large. Figure 13 presents, for fixed $kh/2\pi = 1$, the wave speed and attenuation vs plate thickness. Correlated with Fig. 12,

we observe from Fig. 13 that (1) when the plate thickness is less than a certain value, both the wave speed and attenuation are independent of the thickness for all the three modes; (2) with further increasing plate thickness, the wave speed decreases from the PE Lamb wave in the PE ZnO plate to that in the corresponding elastic ZnO plate; (3) with further increasing plate thickness, the wave attenuation decreases first and then increases. The critical plate thickness for these sharp changes is 4.074 mm [$\log(h) = -2.39 \text{ m}$], 5.888 mm [$\log(h) = -2.23 \text{ m}$], and 7.413 mm [$\log(h) = -2.13 \text{ m}$], respectively, for the first, second, and third modes. We point out that, similar to the SH wave in Fig. 6(b), once a wave mode is selected, the critical PSC plate thickness should be avoided.

4. Effect of biasing electric fields on wave speed and attenuation

The dispersion and attenuation curves of the first three modes for different horizontal biasing electric field α with fixed $n_0 = 1 \times 10^{15} \text{ m}^{-3}$, $h = 1 \text{ mm}$, and $\bar{E}_3 = 0$ are shown in Fig. 14. It is observed from Fig. 14, that while the biasing electric field α has nearly no influence on the wave speed, it affects the wave attenuation substantially. Figure 15 shows the variation of the wave speed and attenuation of the first three modes with α . With increasing wavenumber, the wave attenuation changes its sign when α is at a critical value around 0.2. We further notice that the effect of α on the Lamb wave speed and attenuation is similar to that on the SH wave [Fig. 8(b)]. This indicates that the Lamb wave can be also amplified by applying a horizontal biasing electric field when the electrons drift velocity is larger than the Lamb wave velocity.⁶

For fixed $n_0 = 1 \times 10^{15} \text{ m}^{-3}$, $h = 1 \text{ mm}$, and $\bar{E}_1 = 0$, Figs. 16 and 17 (also with fixed $kh/2\pi = 1$) show the wave speed and

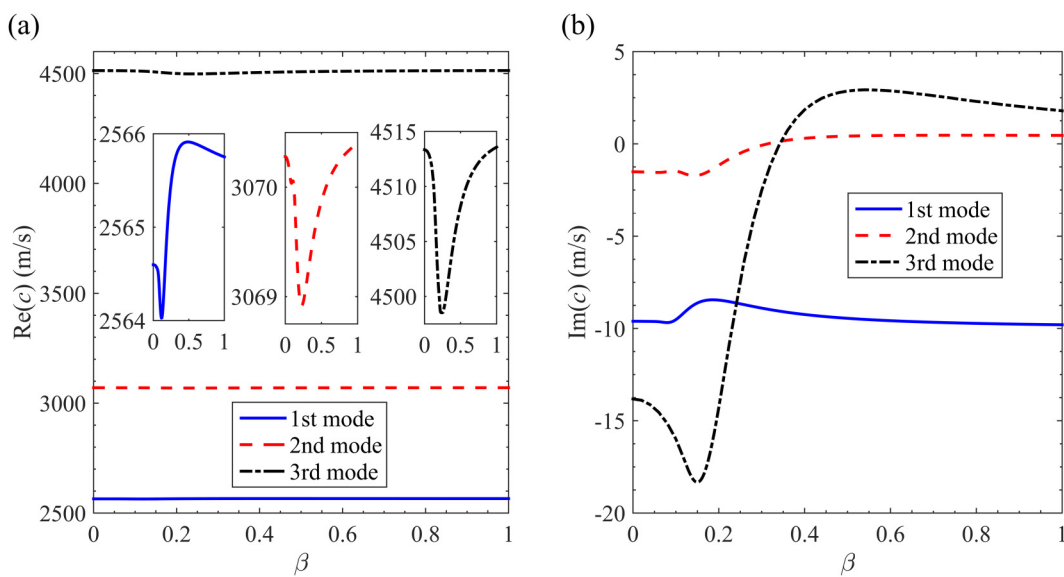


FIG. 17. Variation of the wave speed and attenuation of the first three modes with the vertical biasing electric field β for fixed $kh/2\pi = 1$. (a) Wave speed and (b) wave attenuation.

attenuation vs wavenumber under different vertical biasing electric field β . Compared with Figs. 14 and 15, it is seen that the effect of β on the wave speed is similar to that of α . Namely, β has nearly no effect on the wave speed. As for the wave attenuation [Fig. 17(b)], the imaginary part becomes positive (corresponding to wave amplification) only on the higher (third) mode and only when the applied vertical biasing electric field is relatively large ($\beta \approx 0.5$ for the largest positive imaginary part). This indicates that, in order to achieve an amplified wave in the PSC plate, applying a horizontal biasing electric field is more efficient than a vertical field.

V. CONCLUSIONS

By introducing the extended Stroh formalism, the analytical formulation for the elastic wave propagation in an anisotropic n-type PSC plate is derived. The extended displacements and stresses of the elastic wave are obtained in terms of the extended Stroh eigenvalues and eigenmatrices. Based on these analytical solutions, the SH and Lamb waves in a transversely isotropic ZnO PSC plate are selected to investigate the influence of the boundary condition, steady-state carrier density, plate thickness, and biasing electric field on the dispersion and attenuation curves. The following important features are observed from our numerical simulation.

- (1) With increasing wavenumber, the SH wave speed of the first two modes approaches the B-G surface wave speed or body shear-wave speed of the PE half-space (depending on the applied boundary condition), and the Lamb wave speed of the first two modes approaches the Rayleigh wave speed of the PE half-space (again depending on the applied boundary condition).
- (2) Contrary to the elastic waves in the elastic or PE plate, the dispersion and attenuation curves in a PSC plate depend on the plate thickness. Furthermore, waves in the PSC medium are dissipative.
- (3) For a fixed plate thickness (i.e., $h = 1$ mm), when the steady-state carrier density is small ($n_0 < 1 \times 10^{12} \text{ m}^{-3}$), the wave characteristics in the PSC plate are the same as that in the corresponding PE plate; when $n_0 > 1 \times 10^{20} \text{ m}^{-3}$, the wave characteristics then are the same as that in the corresponding elastic plate; within the range $1 \times 10^{12} \text{ m}^{-3} < n_0 < 1 \times 10^{20} \text{ m}^{-3}$, n_0 can significantly affect the wave speed and attenuation. More specifically, with increasing n_0 , the wave speed decreases, and the wave attenuation decreases first and then increases. In other words, the steady-state (or initial) carrier density is one of the key parameters which should be fully analyzed when designing a PSC device.
- (4) For a given n_0 (e.g., $n_0 = 2 \times 10^{15} \text{ m}^{-3}$), with increasing plate thickness, the wave in the PSC plate first propagates with the wave speed in the corresponding PE plate; it then decreases and eventually propagates with the wave speed in the corresponding elastic plate; as for the wave attenuation, it increases first and then decreases with increasing plate thickness. In other words, the plate thickness is the other key parameter which should be considered when designing a PSC device.
- (5) With increasing biasing electric field, the wave speed in the PSC plate decreases first and then increases. When the biasing electric field is larger than a fixed (critical) value, the wave

attenuation changes its sign so that the wave amplitude increases instead of decreases. However, wave amplification can be achieved relatively easily by applying a horizontal biasing field, as compared to that by applying a vertical field.

- (6) In summary, critical values (for the change of steady-state carrier density, the plate thickness, and biasing electric field) exist at which the maximum wave attenuation can be achieved.

ACKNOWLEDGMENTS

This work was supported by the National Natural Science Foundation of China (NNSFC) (Grant Nos. 11472182 and 11272222). A. K. Soh was supported by the 2017 Monash University Malaysia Strategic Large Grant Scheme (Project Code No. LG-2017-04-ENG).

APPENDIX A: THE ELEMENTS OF MATRIX [M]

In order to list the elements of matrix [M] in Eq. (23), we first define the following matrix [P]:

$$[P]_{20 \times 10} = \begin{bmatrix} E_{11}\langle e^{-ikhs_-} \rangle & E_{12} \\ ikE_{21}\langle e^{-ikhs_-} \rangle & ikE_{22} \\ E_{11} & E_{12}\langle e^{ikhs_+} \rangle \\ ikE_{21} & ikE_{22}\langle e^{ikhs_+} \rangle \end{bmatrix}.$$

The elements of matrix [M] in Eq. (23) are expressed as

$$\begin{aligned} M(1:5; 1:10) &= P(4:8; 1:10), \\ M(6:10; 1:10) &= P(14:18; 1:10), \end{aligned}$$

for electrically shorted case and

$$\begin{aligned} M(1:4; 1:10) &= P(5:8; 1:10), \\ M(5:8; 1:10) &= P(15:18; 1:10), \\ M(9; 1:10) &= -ikP(9; 1:10) + P(10; 1:10), \\ M(10; 1:10) &= -ikP(19; 1:10) + P(20; 1:10), \end{aligned}$$

for electrically open case 1 and

$$\begin{aligned} M(1:4; 1:10) &= P(5:8; 1:10); \\ M(5:8; 1:10) &= P(15:18; 1:10); \\ M(9; 1:10) &= -ikP(9; 1:10) + P(10; 1:10) + ik^2\epsilon_0 P(4; 1:10); \\ M(10; 1:10) &= -ikP(19; 1:10) + P(20; 1:10) - ik^2\epsilon_0 P(14; 1:10) \end{aligned}$$

for electrically open case 2.

REFERENCES

- ¹A. Janotti and C. G. Van de Walle, *Rep. Prog. Phys.* **72**, 126501 (2009).
- ²B. Kumar and S. W. Kim, *J. Mater. Chem.* **21**, 18946 (2011).
- ³Z. L. Wang, *Adv. Mater.* **24**, 4632 (2012).
- ⁴A. R. Hutson and D. L. White, *J. Appl. Phys.* **33**, 40 (1962).
- ⁵B. A. Auld, *Acoustic Fields and Waves in Solids* (John Wiley and Sons, New York, 1973), p. 357.
- ⁶D. L. White, *J. Appl. Phys.* **33**, 2547 (1962).

- ⁷S. Ghosh and P. Khare, Ind. J. Pure Ap. Phys. **44**, 183 (2006), available at <http://nopr.niscair.res.in/handle/123456789/8259>.
- ⁸M. Willatzen and J. Christensen, Phys. Rev. B **89**, 041201 (2014).
- ⁹P. X. Gao, J. H. Song, J. Liu, and Z. L. Wang, Adv. Mater. **19**, 67 (2007).
- ¹⁰J. H. Kang, D. K. Jeong, J. S. Ha, J. K. Lee, and S. W. Ryu, Semicond. Sci. Technol. **32**, 025001 (2017).
- ¹¹Y. Purusothaman, N. R. Alluri, A. Chandrasekhar, and S. J. Kim, Nano Energy **50**, 256 (2018).
- ¹²F. J. R. Schülein, K. Müller, M. Bichler, G. Koblmüller, J. J. Finley, A. Wixforth, and H. J. Krenner, Phys. Rev. B **88**, 085307 (2013).
- ¹³S. Büyükköse, A. Hernández-Mínguez, B. Vratzov, S. Somaschini, L. Geelhaar, H. Riechert, W. G. van der Wiel, and P. V. Santos, Nanotechnology **25**, 135204 (2014).
- ¹⁴R. M. White, IEEE T. Electron Dev. **14**, 181 (1967).
- ¹⁵J. S. Yang and H. G. Zhou, Int. J. Solids Struct. **42**, 3171 (2005).
- ¹⁶J. S. Yang, X. M. Yang, and J. A. Turner, Arch. Appl. Mech. **74**, 288 (2004).
- ¹⁷C. L. Gu and F. Jin, Philos. Mag. Lett. **95**, 92 (2015).
- ¹⁸F. Y. Jiao, P. J. Wei, Y. H. Zhou, and X. L. Zhou, Eur. J. Mech. A Solid **75**, 70 (2019).
- ¹⁹F. Y. Jiao, P. J. Wei, X. L. Zhou, and Y. H. Zhou, Ultrasonics **92**, 68 (2019).
- ²⁰J. H. Collins, K. M. Lakin, C. F. Quate, and H. J. Shaw, Appl. Phys. Lett. **13**, 314 (1968).
- ²¹D. R. Dietz, L. J. Busse, and M. J. Fife, IEEE Trans. Ultrason. Ferroelectr. Freq. Control **35**, 146 (1988).
- ²²J. S. Yang and H. G. Zhou, Acta Mech. **176**, 83 (2005).
- ²³J. S. Yang and H. G. Zhou, Int. J. Appl. Electrom. **22**, 97 (2005).
- ²⁴J. S. Yang and H. G. Zhou, J. Zhejiang Univ. Sci. **6A**, 90 (2005).
- ²⁵J. N. Sharma, K. K. Sharma, and A. Kumar, J. Mech. Mater. Struct. **6**, 791 (2011).
- ²⁶J. N. Sharma, K. K. Sharma, and A. Kumar, World J. Mech. **1**, 247 (2011).
- ²⁷K. Shintani and H. Itoh, Int. J. Eng. Sci. **32**, 1271 (1994).
- ²⁸D. M. Barnett and J. Lothe, Phys. Status Solidi B **67**, 105 (1975).
- ²⁹E. Pan, Z. Angew. Math. Phys. **53**, 815 (2002).
- ³⁰F. Zhu, B. Wang, Z. H. Qian, and E. Pan, Int. J. Solids Structures **150**, 52 (2018).
- ³¹E. Pan and W. Q. Chen, *Green's Functions in Anisotropic Media* (Cambridge University Press, New York, 2015).
- ³²D. J. Yan, A. L. Chen, Y. S. Wang, C. Zhang, and M. Golub, Int. J. Mech. Sci. **142-143**, 276 (2018).
- ³³H. F. Tiersten and T. L. Sham, IEEE Trans. Ultrason. Ferroelectr. Freq. Control **45**, 1 (1998).
- ³⁴L. Qin, Q. Chen, H. Cheng, and Q. M. Wang, IEEE Trans. Ultrason. Ferroelectr. Freq. Control **57**, 1840 (2010).
- ³⁵L. Qin, Q. Chen, H. Cheng, Q. Chen, J. F. Li, and Q. M. Wang, J. Appl. Phys. **110**, 094511 (2011).
- ³⁶J. L. Bleustein, Appl. Phys. Lett. **13**, 412 (1968).
- ³⁷Y. V. Gulyaev, Sov. Phys. JETP Lett. **9**, 37 (1969).
- ³⁸A. R. Hutson, J. H. Mcfee, and D. L. White, Phys. Rev. Lett. **7**, 237 (1961).
- ³⁹K. Moon, I. M. Le, J. H. Shin, E. S. Lee, N. Kim, W. H. Lee, H. Ko, S. P. Han, and K. H. Park, Sci. Rep. **5**, 13817 (2015).